# Electrical Connectivity in Single-Walled Carbon Nanotube Networks

**ARTICLE** *in* NANO LETTERS · SEPTEMBER 2009

Impact Factor: 13.59 · DOI: 10.1021/nl9020914 · Source: PubMed

NANO LETTERS

2009
Vol. 9, No. 11
3890-3895

# Electrical Connectivity in Single-Walled Carbon Nanotube Networks

**Peter N. Nirmalraj,[†,§] Philip E. Lyons,[‡,§] Sukanta De,[‡,§] Jonathan N. Coleman,[‡,§] and John J. Boland*[,†,§]**

*School of Chemistry, School of Physics, Center for Research on Adaptive Nanostructures and Nanodevices (CRANN), Trinity College Dublin, Dublin 2, Ireland*

*Received June 30, 2009; Revised Manuscript Received September 1, 2009*

## ABSTRACT

**Transport in single-walled carbon nanotubes (SWCNTs) networks is shown to be dominated by resistance at network junctions which scale with the size of the interconnecting bundles. Acid treatment, known to dope individual tubes, actually produces a dramatic reduction in junction resistances, whereas annealing significantly increases this resistance. Measured junction resistances for pristine, acid-treated and annealed SWCNT bundles correlate with conductivities of the corresponding films, in excellent agreement with a model in which junctions control the overall network performance.**

Since the pioneering work of Iijima,[1] it has been recognized that carbon nanotubes have potential applications in nanoscale electronics[2] and biological sensing.[3,4] Field-effect transistors based on individual semiconducting single-walled carbon nanotubes (SWCNTs) and interconnects based on metallic SWCNTs have been demonstrated.[5] However, for devices comprised of individual tubes controlling the chirality and material placement remains a challenge. Nanotube networks (NTNs) on the other hand are easier to mass produce and drawbacks associated with variations in electronic properties of individual tubes are averaged out within a network, making NTNs promising candidates in applications ranging from thin film transistors[6] to flexible displays.[7−18] The latter application has received a lot of attention in recent years due to the potential for NTNs to replace indium tin oxide as a transparent electrode material. Nanotube films have the added advantage that they are flexible,[10,11] making them ideal for applications such as electronic paper.

To function as a transparent conductor, NTNs must have sheet resistance, $R_s$, of <100 Ω/□ coupled with optical transmittance, $T$, of >90% (generally taken at 550 nm). Sheet resistance and transmittance are related by[19]

$$T(\lambda) = \left(1 + \frac{188.5}{R_s}\frac{\sigma_{Op}(\lambda)}{\sigma_{DC}}\right)^{-2} \quad (1)$$

where $\sigma_{DC}$ and $\sigma_{Op}$ are the DC and optical conductivities, respectively. The required properties (low $R_s$, high $T$) are achieved for high values of the ratio $\sigma_{DC}/\sigma_{Op}$. As $\sigma_{Op}$ is generally close to $1.7 \times 10^4$ S/m for nanotube films[11,20,21] the problem reduces to maximizing $\sigma_{DC}$. While DC conductivity depends on the network morphology,[22] the most important factor determining network conductivity is believed to be the intertube electron transfer at nanotube−nanotube junctions.[22]

Geometrical scaling arguments[22−24] have shown that the conductivity, $\sigma_{DC}$, of disordered nanotube films scales linearly with the number density of network junctions, $N_j$, which in turn scales with the network morphology though the film fill-factor, $V_f$, the mean diameter, $\langle D\rangle$, of the bundles and the mean junction resistance, $\langle R_J\rangle$

$$\sigma_{DC} = \frac{K}{\langle R_J\rangle}\frac{V_f^2}{\langle D\rangle^3} \quad (2)$$

Here $K$ is the proportionality factor that scales with the bundle length as a separate analysis recently revealed that $\sigma \propto L^{1.7}$.[23] Equation 2 predicts that the network conductivity scales inversely with the mean junction resistance. Thus, understanding the electrical properties of junctions is critical to the development of highly conducting nanotube films. To do this, local investigation of the electrical properties of NTNs is required.

Previously, conductance atomic force microscopy (C-AFM) was used by Fujiwara et al.,[25,26] Stadermann et al.,[27,28] Pablo et al.,[29] and Rispal et al.[30] to study the local electronic properties of individual bundles in SWCNT networks. These studies did not examine in detail the dependence of the local

* To whom correspondence should be addressed. Phone: 003531896 3140. Fax: 003531896 3142. E-mail: jboland@tcd.ie.
† School of Chemistry, Trinity College.
‡ School of Physics, Trinity College.
§ Center for Research on Adaptive Nanostructures and Nanodevices (CRANN), Trinity College.

10.1021/nl9020914 CCC: $40.75 
**Published on Web 09/23/2009**

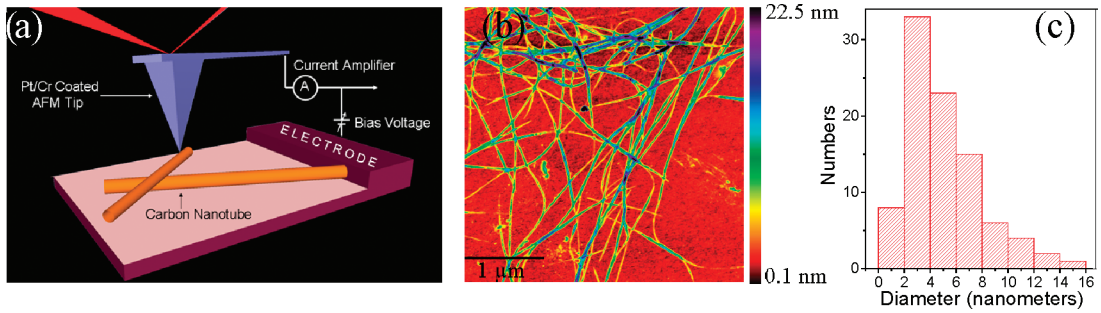


**Figure 1.** (a) Schematic of conductive atomic force microscope technique. (b) Morphology of NTN showing the presence of both individual nanotubes and nanotubes bundles forming networks deposited using SWCNT concentration of 0.025 mg/mL. (c) The bundle diameter histogram shows the presence of individual tubes and a larger population of nanotube bundles.

resistance at junctions on the diameter of constituent tubes, although Stadermann et al.[28] highlighted that increases in resistance in NTNs coincided with junction locations. Here, the intrinsic conductivity of individual SWCNTs and SWCNT bundles and the junction resistance between individual tubes and bundles have been analyzed. We demonstrate that the junction resistance is strongly dependent on the size of the interconnecting bundles. Moreover, acid treatment commonly used to dope SWCNTs actually results in a significant lowering of the resistance at network junctions. Dedoping by high-temperature annealing produced more resistive junctions and films. Finally, we link the junction resistance to the conductivity of bulk films and in doing so demonstrate the validity of the transport model described by Equation 2.

Sparse NTNs were formed by spray coating SWCNTs (Iljin Nanotech arc discharge tubes) dispersed in *N*-methyl-pyrollidone (NMP) onto $SiO_2$ substrates and subsequently annealed in argon at 500 °C for 5 h in order to remove the adsorbed solvent. Our Dimension V AFM was operated in the C-AFM mode, in which the AFM tip acts like a mobile nanocontact that is held at ground potential with a DC bias applied to the sample (see Figure 1A). The force feedback signal is used to generate a normal contact mode AFM topographic image and the current passing between the conducting cantilever (ContE with chromium/platinum coating from Budget Sensors with a force constant of 0.2 N/m and a resonant frequency of 13 kHz) and the sample simultaneously generates the conductance image. Typical bias voltages of 0.2 mV to 1 V resulted in currents of 2pA to 1 $\mu$A. Figure 1B shows the morphology of a typical NTN as analyzed by AFM and is found to comprise of a mixed population of tubes with varying diameters (see Figure 1c). A separate STM study revealed that single Iljin tubes have diameters between 1.2 to 1.8 nm, whereas from AFM measurements of individual tubes we calculate a mean diameter and length of 1.6 nm and 1.5 $\mu$m, respectively. This demonstrates that the dispersion method used to produce the sparse NTN in Figure 1b is effective in generating a significant population of individual tubes and small diameter bundles,[31] which are key properties for the formation of highly conductive NTN films.

Since C-AFM is a two terminal measurement, it is not possible to eliminate the contribution from the resistance at the contacts (electrode and AFM probe). However, comparisons can still be made provided the contacts are stable, which is guaranteed by measuring a low resistance (~300 Ω) when the probe directly contacts the electrode and by applying the same probe force during all current measurements. The networks studied were very sparse and intentionally selected such that there are no back-door connections to the electrode (see Supporting Information).

Figure 2a shows a current map of a region of network and 2c shows a schematic detailing the tube size and junction geometry, the latter being determined from high resolution topography maps (see Supporting Information). Note the width of the current trace is not reflective of the actual diameter of the tube. The current map was converted into a resistance measurement along the two traces shown. Pathway 1 is traced from the electrode along a ~2.3 nm tube bundle, until it encounters a ~1.65 nm single tube, which is lying on top of the bundle, and then the trace continues along the bundle again. The resistance increases monotonically along the bundle until the junction with the single tube at which point there is a jump and after which it recovers to the original level.

From data like these we can get two types of information; analysis of the rate of increase of resistance with position along the bundle gives us the effective bundle conductivity, while the magnitude of the jump at the junction tells us about the junction resistance. Treating the bundle as a resistive cylinder connected via the rest of the network to the electrode we can write the bundle resistance, $R$, as

$$R = R_{\text{other}} + \frac{l}{\sigma_{\text{bun}} A} \tag{3}$$

Here $R_{\text{other}}$ is the combined resistance of the network and contacts, $l$ is the position along the bundle, while $\sigma_{\text{bun}}$ and $A$ are the bundle conductivity and cross-sectional area respectively. By measuring d$R$/d$l$, we calculate the conductivity of the ~2.3 nm bundle to be ~$3 \times 10^6$ S/m. This is in good agreement with measurements on individual ropes of SWNTs, which gives conductivity close to $10^6$ S/m.[32] In comparison, measurements on well graphitised individual MWNTs gives values of $\sigma = 8 \times 10^6$ S/m.[33] Note however, that the measured conductivity of the bundle is a lower bound since not all of the tubes within the bundle cross-section may contribute to the measured current.

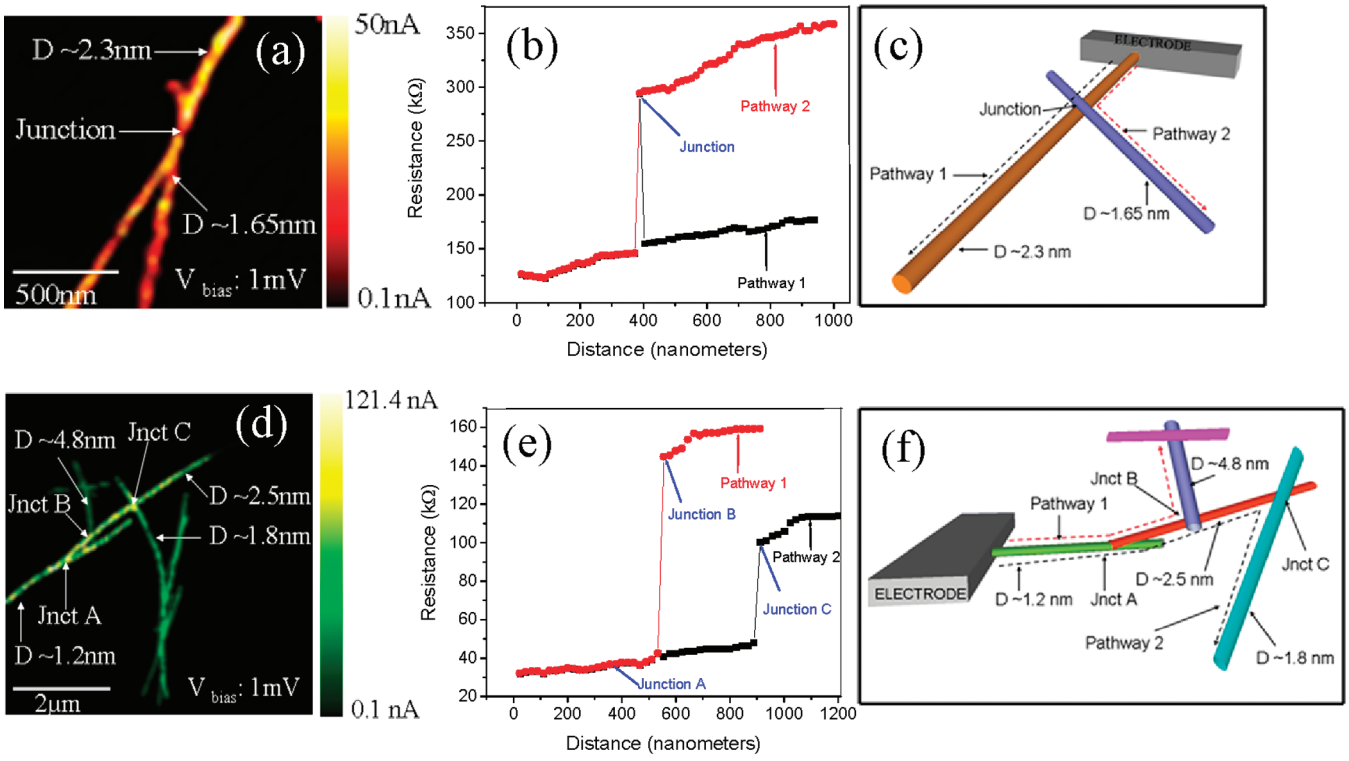


**Figure 2.** C-AFM results on pristine Iljin sparse networks. (a) Current map of a nanotube bundle ($D \sim 2.3$ nm), which is intersected by an individual tube ($D \sim 1.65$ nm). The electrode is positioned on the top of the image (not shown). (b) Local resistance analysis through the bundle and individual tube depicted as pathway 1 and 2 as shown in the schematic (c). (d) Current map of interconnected tubes of varying diameter showing the formation of junctions with varying resistances. (e) Local resistance analyzed along the individual tube connected to a sparse configuration of nanotubes highlighted as pathway 1 and 2 as shown in the schematic in (f). The electrode is positioned on the left-hand side of the image (not shown). (CI-AFM scanning parameters for a and d: bias Voltage 1 mV, preamplifier sensitivity 100 nA/V.)

The observed jump in resistance of ~180 kΩ corresponds to the resistance of the junction between the bundle and the single tube. Along pathway 1 we see a spike in the resistance as the AFM tip momentarily passes over the single tube. For pathway 2, the resistance increases abruptly and then remains constant. This is due to the tip initially following the bundle before moving to and subsequently following the single tube. In each case, the resistance change is equal to the junction resistance between a ~2.3 nm bundle and a ~1.65 nm single tube.

Figure 2d shows a more complex section of network comprised of two single tubes and two bundles, which intersect to create three different junctions (labeled A−C), also a zoomed out current map relevant to Figure 2d is attached in the Supporting Information to show that the networks analyzed are very sparse and measurements are specifically targeted toward areas where only a single tube is connected to the electrode, and the rest of the tubes branch out from that single tube.

Two pathways are traced along this network involving junctions A, B, and C. Pathway 1 shows a ~1.2 nm single tube whose resistance slowly increases as the single tube merges into a smaller diameter bundle (~2.5 nm) at junction A. The absence of a marked increase in resistance beyond junction A reflects an intimate contact between the single tube along the length of the bundle (see Supporting Information) and suggests that both are metallic. The resistance increase along the single tube indicates a conductivity of $\sim 6.7 \times 10^7$ S/m, significantly higher than that observed for the ~2.3 nm bundle. There is a sharp increase in resistance (~115 kΩ) at junction B between the ~2.5 nm bundle and the larger diameter bundle (~4.8 nm). Along pathway 2, the ~2.5 nm bundle forms junction C with a ~1.8 nm diameter single tube. The junction resistance is ~70 kΩ, significantly less than the resistance observed between the same ~2.5 nm bundle and the large ~4.8 nm diameter bundle. Evidently, the measured junction resistance is dependent on the diameters of the tubes and bundles comprising the junction.

Figure 3, panel I, summarizes the analysis of hundreds of NTN junctions. The measured resistance values can be separated into one of the four groups, each characterized by the diameter of the tubes forming the junctions. The binning process does not separate metallic and semiconducting elements in these NTNs. We will report separately on back-gating experiments that distinguish between the metallic and semiconducting elements in these NTNs.[28,34,35] The lowest resistance group (labeled A in all panels) has a mean value of 98 kΩ and corresponds to junctions comprised of single nanotubes (1.2−1.8 nm). Junctions formed between single tubes and small diameter bundles (2.5−4.5 nm) (B) have a mean resistance of 230 kΩ, whereas junctions involving exclusively medium (4.5−6.8 nm) and larger diameter bundles (7−14 nm) have resistances of 294 kΩ (C) and 2.7 MΩ (D), respectively. We have also measured the mean

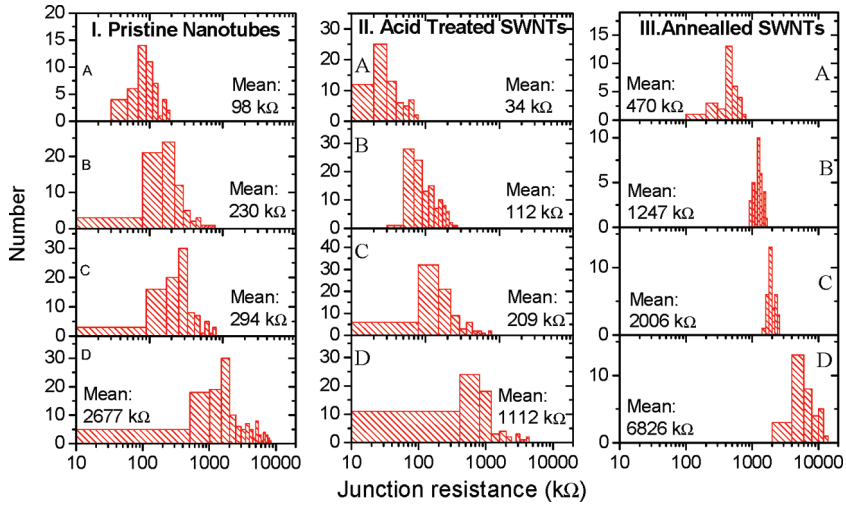


**Figure 3.** Diameter dependent junction resistance analysis. Junction resistance analysis of pristine (I), acid-treated Ilgin tubes (II) and annealed (III) based on the diameter of the participating tubes. Case A, B, C, and D in the three panels are the junction resistance measured between individual tubes (diameter, 1.2−1.8 nm), between individual nanotubes and smaller diameter nanotube bundles (diameter, 2.5−4.5 nm), between smaller diameter nanotube bundles (diameter, 4.5−6.8 nm) and the junction resistance between larger diameter nanotube bundles (diameter, 7−14 nm), respectively.

conductivity associated with individual SWCNTs to be (4.4 ± 1.6) × $10^7$ S/m (averaging over ∼30 semiconducting and metallic tubes).

This trend in junction resistances has not been previously reported but can be understood in terms of the resistances that exist between individual tubes within a bundle. Thus the sharp increase in resistance is a direct measure of the junction resistance only for the case of junctions between individual SWCNTs. For bundles the measured jump in resistance is actually comprised of the two resistances in series: the contact resistance between the bundles $R_C$ and the resistor network associated with charge transport across the bundles $R_B$. The latter depends on the bundle conduction mechanism and we consider here two limiting cases, (i) transport has contributions from all the tubes in the bundle, and (ii) transport is confined to the tube into which charge injection occurs. Since C-AFM is restricted to measurements at the top surfaces of bundles, it measures $R_C + R_D$, where $R_D$ is the resistor network associated with transport across the entire diameter of the bundle. For case (i), since $R_B \leq R_D$ the measured resistance jump is an upper bound on the true junction resistance $R_J = R_C + R_B$. For case (ii), the value of $R_B$ depends on the precise location of the tubes that carry charge in and out of the junction. At one extreme, we consider the two tubes that make physical contact at the junction, in which case $R_B = 0$ and hence $R_J = R_C$. Alternatively, the tubes could be on the opposite sides of the two bundles that comprise the junction so that $R_B = 2 \times R_D$. Therefore, for case (ii) the junction resistance is bounded by $R_C \leq R_J \leq (R_C + 2 \times R_D)$, and thus the average value is well described by the measured resistance jump of $R_C + R_D$. This analysis shows that C-AFM provides a good measure of junction resistance and that effective debundling and hence smaller $R_B$ values is critical in the formation of highly conducting NTNs.

Acid treatment is known to enhance the conductivity of carbon nanotube materials and is widely used in the production of NTNs. To examine the influence of acid treatment on the junction resistance, Iljin mats were exposed to nitric acid (70%, 15 M) for 2 h at room temperature, followed by vacuum filtration and rinsing with deionized water. These materials were dispersed and spray deposited as described earlier. Panel II in Figure 3 shows the junction resistance values for the resulting NTNs. Remarkably, we find that in each case the junction resistance is reduced over that of the pristine tubes. The largest reduction is observed for junctions comprised of single tubes, where a 3-fold drop is observed. Previous studies, have shown that acid treatment results in doping[36,37] and for nanotube films the conductivity typically increases by four times.[14] Here, we find that the intrinsic conductivity of individual acid-treated nanotubes increased slightly compared to individual pristine SWCNTs, $\sigma_{acid} = (5.6 \pm 1.2) \times 10^7$ S/m compared to $\sigma_{pristine} = (4.4 \pm 1.6) \times 10^7$ S/m. This shows that acid treatment only results in a small increase (∼30%) in tube conductivity. Evidently, increases in film conductivity attributed to acid treatment have much more to do with a 3-fold reduction in junction resistance rather than a 30% increase in the conductivity of the interconnecting tubes.

Having shown how acid treatment affects the junction resistance, we might expect a related effect after annealing. We annealed a pristine NTN film in argon at 1000 °C for 12 h, conditions that have been shown in the literature to dedope SWNTs.[38−41] Figure 4a shows the current map of a junction formed between two annealed tubes, a small diameter bundle (∼2.2 nm) and an individual tube (∼1.6 nm). The resistance trace along the bundle indicates an effective conductivity of ∼1 × $10^6$ S/m, which should be compared with ∼3 × $10^6$ S/m previously observed for a ∼2.3 nm unannealed pristine bundle. Clearly, annealing has decreased the tube conductivity by a factor of 3, consistent with dedoping. However, the measured resistance jump at the junction is ∼1.3 MΩ. This large value is representative of these annealed samples and can be compared with the

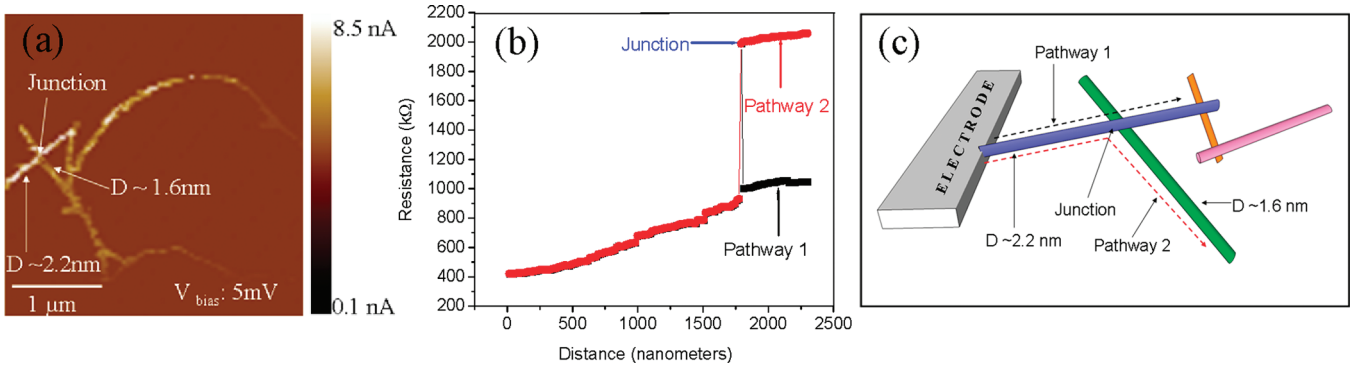


**Figure 4.** Junction resistance analysis of annealed tubes. (a) Current map of a smaller diameter bundle, ($D \sim 2.2$ nm) connected to the electrode on the left-hand side of the image (not shown) and intersected by an individual tube ($D \sim 1.6$ nm). (b) The plot shows the resistance to increase by ~1.3 MΩ at the junction point. Pathway 1 and pathway 2 shown in 4b is the resistance traced along the bundle and the resistance traced from the bundle through the interconnecting individual tube as depicted in the schematic (c). The electrode is positioned on the left-hand side of the image (not shown). (CI-AFM scanning parameters, bias Voltage 5 mV, preamplifier sensitivity 100 nA/V.)

~230 and 112 kΩ junction values typically found between single tubes and smaller diameter bundles in pristine and acid-treated NTNs, respectively (see Figure 3). A histogram of junction resistances in sparse NTNs after annealing is shown in panel III. As with acid treatment, although annealing modulates the resistivity of the interconnecting tubes, it has a more marked influence on the resistance of the interconnecting junctions.

Following this analysis of intertube and interbundle junctions, we can test whether these observations are consistent with the model described by eq 2, which predicts that the nanotube film conductivity scales inversely with the mean junction resistance. To do this we make films of the sort typically used as transparent conductors using pristine, acid-treated and annealed nanotubes (see Supporting Information). For pristine films we measured the sheet resistance to be ~110 Ω/□ for films on both PET and quartz. Optical transmittance measurements gave values of ~78% ($\lambda = 550$ nm) for films on both substrates. Using eq 1, we can calculate that these $R_s$ and $T$ values imply a value of $\sigma_{DC}/\sigma_{Op} \approx 13$. This value is comparable to the best performance reported for untreated nanotube networks.[11,15] Taking $\sigma_{Op} = 1.7 \times 10^4$ S/m, we calculate $\sigma_{DC} \approx 2.2 \times 10^5$ S/m for both substrates. In the case of acid-treated films, we measured sheet resistance and transmittance on PET to be 37 Ω/□ and 76%, respectively. This corresponds to values of $\sigma_{DC}/\sigma_{Op} = 35$ and $\sigma_{DC} = 6 \times 10^5$ S/m. We note that these values are extremely high and compare favorably with the best films produced to date.[14,18] In addition, $\sigma_{DC}/\sigma_{Op} = 35$ represents the critical value above which, T > 90% and $R_S$ < 100 Ω can be attained (see eq 1). Thus, this work is the first demonstration of a nanotube network that meets the minimum industry standards for a transparent conductor. Finally for annealed films, we measured the sheet resistance and transmittance of 285 Ω/□ and 79% respectively. This corresponds to values of $\sigma_{DC}/\sigma_{Op} = 5.3$ and $\sigma_{DC} = 9 \times 10^4$ S/m. The annealed films are less conductive than pristine or acid-treated films.

Given measurements for both junction resistance and film conductivity for pristine, acid-treated and annealed NTNs,

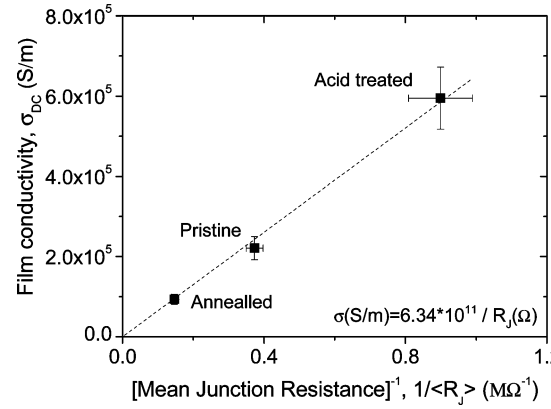


**Figure 5.** Plot of measured film conductivity as a function of the inverse of mean junction resistance measured for pairs of larger bundles (see panels ID, IID, and IIID in Figure 3). The error in junction resistance is the standard error of the distribution while the error in film resistivity is associated with the calculation of the film thickness.

we can test the inverse relationship predicted by eq 2. We use the conductivities for the pristine, acid-treated and annealed films discussed above. We take the mean junction resistance for the large bundle junctions (D in panels I, II and III). This is because the thicker films used for conductivity measurements tend to have higher bundle diameters ($\langle D \rangle \sim 20$ nm). We plot this data in Figure 5, as film conductivity versus the inverse of mean junction resistance,$1/\langle R_J \rangle$. We find a near perfect linearity, indicating very good agreement between experiment and model. This shows categorically that film properties are controlled by the junctions. In addition, it demonstrates that while both nanotube/bundle conductivity are affected by treatments such as acid treatment and annealing, it is the change in junction resistance that controls the film conductivity.

This work conclusively demonstrates the critical role of debundling in controlling the conductivity of nanotube films. It is known that by reducing the bundle diameter, the junction density increases and with it the number of pathways for charge transport.[22] The present data show that decreasing the bundle diameter also reduces the junction resistance, thus

increasing the conductivity even further. Additionally, the dominant effect of acid treatment is an unexpected reduction in junction resistance. Although the mechanism is unclear at present, we speculate that the barriers at junctions are related to charge transfer between tubes and that the availability of additional carriers in highly doped tubes effectively screen these electrostatic interactions. Our conclusions are supported by the recent work of Barnes et al.[42] By carrying out temperature dependent electrical measurements on nanotube films, they showed that, in addition to doping, chemical treatment of nanotube films tends to alter the potential barrier at internanotube junctions. This would tend to alter the effective junction resistance as we have demonstrated here.

In summary, we demonstrated that the resistance of NTN junctions is strongly dependent on the diameter of the constituent tubes with the smallest values associated with individual tubes. Additionally, junction resistance can be controlled by acid treatment, and that the dominant effect of doping is a dramatic reduction of the barrier to transport between individual tubes and bundles. Finally, the measured junction resistances for pristine, acid-treated and annealed SWNT bundles correlate with the measured conductivities of the corresponding films, which is in excellent agreement with a simple model in which junctions control the overall network performance.

**Acknowledgment.** We acknowledge the Science Foundation Ireland funded collaboration (SFI Grant 03/CE3/M406s1) between Trinity College Dublin, University College Cork, and Hewlett-Packard, Dublin Inkjet Manufacturing Operation, which allowed this work to take place.

**Supporting Information Available:** The topography data for all the current maps traced is included along with the sample preparation procedure involving pristine, acid-treated, and annealed films. This material is available free of charge via the Internet at http://pubs.acs.org.

## References

(1) Iijima, S. *Nature* **1991**, *354* (6348), 56–58.
(2) Pichler, T.; Knupfer, M.; Golden, M. S.; Fink, J.; Rinzler, A.; Smalley, R. E. *Phys. Rev. Lett.* **1998**, *80* (21), 4729–4732.
(3) Valentini, F.; Orlanducci, S.; Terranova, M. L.; Amine, A.; Palleschi, G. *Sens. Actuators, B* **2004**, *100* (1−2), 117–125.
(4) Allen, B. L.; Kichambare, P. D.; Star, A. *Adv. Mater.* **2007**, *19* (11), 1439–1451.
(5) Avouris, P.; Chen, Z. H.; Perebeinos, V. *Nat. Nanotechnol.* **2007**, *2* (10), 605–615.
(6) Artukovic, E.; Kaempgen, M.; Hecht, D. S.; Roth, S.; GrUner, G. *Nano Lett.* **2005**, *5* (4), 757–760.
(7) Aguirre, C. M.; Auvray, S.; Pigeon, S.; Izquierdo, R.; Desjardins, P.; Martel, R. *Appl. Phys. Lett.* **2006**, *88* (18), 3104.
(8) Barnes, T. M.; Van de Lagemaat, J.; Levi, D.; Rumbles, G.; Coutts, T. J.; Weeks, C. L.; Britz, D. A.; Levitsky, I.; Peltola, J.; Glatkowski, P. *Phys. Rev. B* **2007**, *75* (23), 5410.
(9) Barnes, T. M.; Wu, X.; Zhou, J.; Duda, A.; van de Lagemaat, J.; Coutts, T. J.; Weeks, C. L.; Britz, D. A.; Glatkowski, P. *Appl. Phys. Lett.* **2007**, *90* (24), 3503.
(10) De, S.; Lyons, P. E.; Sorel, S.; Doherty, E. M.; King, P. J.; Blau, W. J.; Nirmalraj, P. N.; Boland, J. J.; Scardaci, V.; Joimel, J.; Coleman, J. N. *ACS Nano* **2009**, *3* (3), 714–720.
(11) Doherty, E. M.; De, S.; Lyons, L.; Shmelov, A.; Nirmalraj, P. N.; Scardaci, V.; Blau, W. J.; Boland, J. J.; Coleman, J. N. *Carbon* **2009**, *47* (10), 2466–73.
(12) Eda, G.; Lin, Y. Y.; Miller, S.; Chen, C. W.; Su, W. F.; Chhowalla, M. *Appl. Phys. Lett.* **2008**, *92* (23), 3305.
(13) Fanchini, G.; Unalan, H. E.; Chhowalla, M. *Appl. Phys. Lett.* **2007**, *90* (9), 2114.
(14) Geng, H. Z.; Kim, K. K.; So, K. P.; Lee, Y. S.; Chang, Y.; Lee, Y. H. *J. Am. Chem. Soc.* **2007**, *129* (25), 7758.
(15) Geng, H. Z.; Lee, D. S.; Kim, K. K.; Han, G. H.; Park, H. K.; Lee, Y. H. *Chem. Phys. Lett.* **2008**, *455* (4−6), 275–278.
(16) Gruner, G. *J. Mater. Chem.* **2006**, *16* (35), 3533–3539.
(17) Parekh, B. B.; Fanchini, G.; Eda, G.; Chhowalla, M. *Appl. Phys. Lett.* **2007**, *90* (12), 1913.
(18) Wu, Z. C.; Chen, Z. H.; Du, X.; Logan, J. M.; Sippel, J.; Nikolou, M.; Kamaras, K.; Reynolds, J. R.; Tanner, D. B.; Hebard, A. F.; Rinzler, A. G. *Science* **2004**, *305* (5688), 1273–1276.
(19) Dressel, M.; Gruner, G. *Electrodynamics of Solids: Optical Properties of Electrons in Matter;* Cambridge University Press: Cambridge 2002.
(20) Hu, L.; Hecht, D. S.; Gruner, G. *Nano Lett.* **2004**, *4* (12), 2513–2517.
(21) Ruzicka, B.; Degiorgi, L.; Gaal, R.; Thien-Nga, L.; Bacsa, R.; Salvetat, J. P.; Forro, L. *Phys. Rev. B* **2000**, *61* (4), R2468–R2471.
(22) Lyons, P. E.; De, S.; Blighe, F.; Nicolosi, V.; Pereira, L. F. C.; Ferreira, M. S.; Coleman, J. N. *J. Appl. Phys.* **2008**, *104* (4), 4302.
(23) Hecht, D.; Hu, L. B.; Gruner, G. *Appl. Phys. Lett.* **2006**, *89* (13), 3112.
(24) Simien, D.; Fagan, J. A.; Luo, W.; Douglas, J. F.; Migler, K.; Obrzut, J. *ACS Nano* **2008**, *2* (9), 1879–1884.
(25) Fujiwara, A.; Iijima, R.; Ishii, K.; Suematsu, H.; Kataura, H.; Maniwa, Y.; Suzuki, S.; Achiba, Y. *Appl. Phys. Lett.* **2002**, *80* (11), 1993–1995.
(26) Fujiwara, A.; Iijima, R.; Suematsu, H.; Kataura, H.; Maniwa, Y.; Suzuki, S.; Achiba, Y. *Physica B* **2002**, *323* (1−4), 227–229.
(27) Stadermann, M.; Papadakis, S. J.; Falvo, M. R.; Fu, Q.; Liu, J.; Fridman, Y.; Boland, J. J.; Superfine, R.; S., W. *Phys. Rev. B* **2005**, *72*, (245406).
(28) Stadermann, M.; Papadakis, S. J.; Falvo, M. R.; Novak, J.; Snow, E.; Fu, Q.; Liu, J.; Fridman, Y.; Boland, J. J.; Superfine, R.; Washburn, S. *Phys. Rev. B* **2004**, *69*, 201402.
(29) de Pablo, P. J.; Martínez, M. T.; Colchero, J.; Gómez-Herrero, J.; Maser, W. K.; Benito, A. M.; Munäoz, E.; Baró, A. M. *Adv. Mater.* **2000**, *12* (8), 573.
(30) Rispal, L.; Stefanov, Y.; Wessely, F.; Schwalke, U. *Jpn. J. Appl. Phys., Part 1* **2006**, *45* (4B), 3672–3679.
(31) Giordani, S.; Bergin, S. D.; Nicolosi, V.; Lebedkin, S.; Kappes, M. M.; Blau, W. J.; Coleman, J. N. *J. Phys. Chem. B* **2006**, *110* (32), 15708–15718.
(32) Fischer, J. E.; Dai, H.; Thess, A.; Lee, R.; Hanjani, N. M.; Dehaas, D. L.; Smalley, R. E. *Phys. Rev. B* **1997**, *55* (8), R4921–R4924.
(33) Wei, B. Q.; Vajtai, R.; Ajayan, P. M. *Appl. Phys. Lett.* **2001**, *79* (8), 1172–1174.
(34) Avouris, P. *Acc. Chem. Res.* **2002**, *35*, 1026–1034.
(35) Tombler, T. W.; Zhou, C. W.; Kong, J.; Dai, H. J. *Appl. Phys. Lett.* **2000**, *76* (17), 2412–2414.
(36) Graupner, R.; Abraham, J.; Vencelova, A.; Seyller, T.; Hennrich, F.; Kappes, M. M.; Hirschb, A.; Ley, L. *Phys. Chem. Chem. Phys.* **2003**, *5*, 5472.
(37) Skakalova, V.; Kaiser, A. B.; Dettlaff-Weglikowska, U.; Hrncarikova, K.; Roth, S. *J. Phys. Chem. B* **2005**, *109* (15), 7174–7181.
(38) Kosaka, M.; Ebbesen, T. W.; Hiura, H.; Tanigaki, K. *Chem. Phys. Lett.* **1995**, *233* (1−2), 47–51.
(39) Musso, S.; Giorcelli, M.; Pavese, M.; Bianco, S.; Rovere, M.; Tagliaferro, A. *Diamond Relat. Mater.* **2008**, *17* (4−5), 542–547.
(40) Vavro, J.; Llaguno, M. C.; Fischer, J. E.; Ramesh, S.; Saini, R. K.; Ericson, L. M.; Davis, V. A.; Hauge, R. H.; Pasquali, M.; Smalley, R. E. *Phys. Rev. Lett.* **2003**, *90* (6), 5503.
(41) Zhou, W.; Vavro, J.; Guthy, C.; Winey, K. I.; Fischer, J. E.; Ericson, L. M.; Ramesh, S.; Saini, R.; Davis, V. A.; Kittrell, C.; Pasquali, M.; Hauge, R. H.; Smalley, R. E. *J. Appl. Phys.* **2004**, *95* (2), 649–655.
(42) Barnes, T. M.; Blackburn, J. L.; van de Lagemaat, J.; Coutts, T. J.; Heben, M. J. *ACS Nano* **2008**, *2* (9), 1968–1976.

NL9020914